Combined action of different mechanisms of convective instability in multilayer systems

Alexander A. Nepomnyashchy and Ilya B. Simanovskii
Department of Mathematics, Technion–Israel Institute of Technology, Haifa 32000, Israel
(Received 26 October 1998)

The nonlinear regimes of convection in a system of three immiscible viscous fluids are investigated by the finite-difference method. We study new phenomena caused by direct and indirect interaction of thermocapillary and buoyancy (Rayleigh and anticonvective) instability mechanisms. Two variants of heating—from below and from above—are considered. The interfaces are assumed to be flat. We focus on nonlinear evolution of steady and oscillatory motions and selection of stable convective structures depending on the parameters of systems. The influence of the lateral boundary conditions is also investigated. A classification of different variants of interaction between Rayleigh and thermocapillary instability mechanisms is presented, and several typical examples are studied. Specifically, we considered six different configurations where the Rayleigh convection arises mainly in a definite layer, and the thermocapillary convection appears mainly near the definite interface. Also, the case where both interfaces are active and alternatively play a dominant role is investigated. Some configurations of interaction between anticonvective and thermocapillary instability mechanisms are considered. [S1063-651X(99)12205-0]

PACS number(s): 47.27.−i, 47.20.−k

I. INTRODUCTION

The phenomenon of Rayleigh-Bénard convection in a horizontal fluid layer between rigid boundaries is caused only by the buoyancy effect. Convection in the presence of *an interface* is characterized by several additional instability mechanisms. The most well-known interfacial physical effect that may cause a convective instability is the *thermocapillary effect* which can generate stationary [1] and oscillatory motions [2–5]. There exists another instability mechanism which appears only in systems with an interface. Although caused by buoyancy, it is nevertheless completely different from the Rayleigh instability mechanism. This kind of instability, which is obtained by heating *from above*, was discovered in [6] and explained from a physical point of view in [7] (see also [8]). This phenomenon, connected essentially with the difference of physical parameters of fluids on both sides of the interface, is called ''anticonvection.''

In a real situation, various instability mechanisms may act simultaneously. The buoyancy instability mechanisms (caused by a *volume* effect) are more important for relatively thick layers, while thermocapillarity (*interfacial* effect) plays the dominant role in the case of thin layers or under microgravity conditions. The combined action of different instability mechanisms may lead to some qualitatively new effects. For instance, competition between two mechanisms of stationary instability can produce oscillations [9].

Recently, some new technologies appeared that are based on complicated multilayer systems, for example, the liquid encapsulation crystal growth technique [10] used in space laboratory missions, which enables the growing crystals to attain a high quality by putting the melt between the fluid layers. The simultaneous interaction of many interfaces with their bulk phases and with each other can lead to a much more complex dynamics and unexpected effects. At present, the combined action of the thermocapillary and buoyancy mechanisms of convection were considered only for the three-layer systems air/silicone oil 50 cs/fluorinert FC70 and air/silicone oil 10 cs/fluorinert FC70 (see [11–13]). For these systems, the thermocapillary and buoyancy forces act in the same direction, and the instability is always stationary near the threshold of the onset of convection.

In the present paper we consider the combined action of several mechanisms of instability for three-layer systems with different physical properties. The paper is organized as follows. In Sec. II we describe the formulation of the problem and the numerical method. Section III is devoted to the consideration of the combined action of Rayleigh and thermocapillary instability mechanisms. In Sec. IV we study the interaction between thermocapillary convection and anticonvection. Section V contains some concluding remarks.

II. FORMULATION OF THE PROBLEM AND NUMERICAL METHOD

Let the rectangular cavity with rigid boundaries be filled by three immiscible viscous fluids (see Fig. 1). The plates are kept at different constant temperatures (the total temperature drop is Θ). It is assumed that surface tension coefficients on the upper and lower interfaces σ and σ_* decrease linearly with temperature: $\sigma=\sigma_0-\alpha T$, $\sigma_*=\sigma_{0*}-\alpha_* T$. In the present paper we do not take into account deformations of the interfaces. Thus, we disregard the long-wavelength deformational instability mode [14,15] which may be observed only in very thin layers with distant lateral boundaries [16]. The linear stability analysis performed for three-layer systems with deformable interfaces [17] shows that the deformational instabilities do not appear in the case of moderate layer lengths. The assumption used does not contradict the results of space experiments [10]. Indices 1 and 3 are related to the exterior layers, and index 2 is related to the middle one.

Let us use the following notations:

$$\nu_*=\nu_3/\nu_1, \quad \nu=\nu_3/\nu_2, \quad \eta_*=\eta_3/\eta_1,$$

 ©1999 The American Physical Society

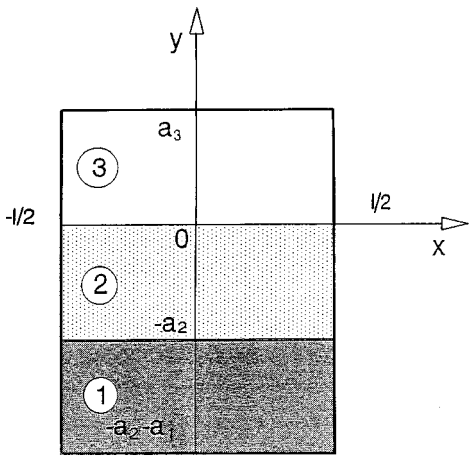

FIG. 1. The system of fluids.

$$\eta=\eta_3/\eta_2,\quad \kappa_*=\kappa_3/\kappa_1,\quad \kappa=\kappa_3/\kappa_2,$$

$$\chi_*=\chi_3/\chi_1,\quad \chi=\chi_3/\chi_2,\quad \beta_*=\beta_3/\beta_1,$$

$$\beta=\beta_3/\beta_2,\quad \overline{\alpha}=\alpha_*/\alpha,$$

$$a_*=a_1/a_3,\quad a=a_2/a_3,\quad L=l/a_3.$$

Here ν_i, η_i, κ_i, χ_i, β_i, and a_i are, respectively, kinematic and dynamic viscosities, heat conductivity, thermal diffusivity, heat expansion coefficient, and thickness of the ith layer ($i=1,2,3$). As the units of length, time, velocity, pressure, and temperature we use a_3, a_3^2/ν_3, ν_3/a_3, $\rho_3\nu_3^2/a_3^2$, and Θ.

Introducing the stream function ψ and the vorticity φ we can write the dimensionless equations in the following form:

$$\frac{\partial\varphi_i}{\partial t}+\frac{\partial\psi_i}{\partial y}\frac{\partial\varphi_i}{\partial x}-\frac{\partial\psi_i}{\partial x}\frac{\partial\varphi_i}{\partial y}=d_i\Delta\varphi_i+b_iG\frac{\partial T_i}{\partial x},$$

$$\Delta\psi_i=-\varphi_i,$$

$$\frac{\partial T_i}{\partial t}+\frac{\partial\psi_i}{\partial y}\frac{\partial T_i}{\partial x}-\frac{\partial\psi_i}{\partial x}\frac{\partial T_i}{\partial y}=\frac{c_i}{P}\Delta T_i\quad (i=1,2,3). \tag{2.1}$$

Here, $d_3=b_3=c_3=1$, $d_1=1/\nu_*$, $b_1=1/\beta_*$, $c_1=1/\chi_*$, $d_2=1/\nu$, $b_2=1/\beta$, $c_2=1/\chi$, $G=g\beta_3\Theta a_3^3/\nu_3^2$ is the Grashof number, and $P=\nu_3/\chi_3$ is the Prandtl number for the liquid in layer 3.

At the interfaces normal components of velocity vanish and the continuity conditions for tangential components of velocity and viscous stresses, temperatures, and heat fluxes also apply: $y=0$:

$$\psi_2=\psi_3=0,\quad \frac{\partial\psi_2}{\partial y}=\frac{\partial\psi_3}{\partial y},\quad T_2=T_3,$$

$$\frac{1}{\kappa}\frac{\partial T_2}{\partial y}=\frac{\partial T_3}{\partial y},\quad \eta\frac{\partial^2\psi_3}{\partial y^2}=\frac{\partial^2\psi_2}{\partial y^2}+Mr\frac{\partial T_3}{\partial x}, \tag{2.2}$$

$y=-a$:

$$\psi_1=\psi_2=0,\quad \frac{\partial\psi_1}{\partial y}=\frac{\partial\psi_2}{\partial y},\quad T_1=T_2$$

$$\frac{1}{\kappa_*}\frac{\partial T_1}{\partial y}=\frac{1}{\kappa}\frac{\partial T_2}{\partial y},\quad \eta_*\eta^{-1}\frac{\partial^2\psi_2}{\partial y^2}=\frac{\partial^2\psi_1}{\partial y^2}+Mr_*\frac{\partial T_2}{\partial x}. \tag{2.3}$$

Here $Mr=\eta M/P$, $Mr_*=\eta_*\overline{\alpha}M/P$, and $M=\alpha\Theta a_3/\eta_3\chi_3$ is the Marangoni number. On the horizontal solid plates the boundary conditions have the form $y=1$:

$$\psi_3=\frac{\partial\psi_3}{\partial y}=0,\quad T_3=0, \tag{2.4}$$

$y=-a-a_*$:

$$\psi_1=\frac{\partial\psi_1}{\partial y}=0,\quad T_1=s, \tag{2.5}$$

$s=1$ for heating from below, $s=-1$ for heating from above.

We consider two kinds of boundary conditions on vertical walls.

(A) Well-conducting boundaries: $x=-L/2,L/2$:

$$\psi_i=\frac{\partial\psi_i}{\partial x}=0,\quad T_i=-A_iy+B_i,\quad i=1,2,3. \tag{2.6a}$$

Here

$$A_1=s\kappa_*(1+\kappa a+\kappa_*a_*)^{-1},\quad A_2=s\kappa(1+\kappa a+\kappa_*a_*)^{-1},$$

$$A_3=s(1+\kappa a+\kappa_*a_*)^{-1},\quad B_1=s\frac{1-(\kappa-\kappa_*)a}{(1+\kappa a+\kappa_*a_*)},$$

$$B_2=B_3=s(1+\kappa a+\kappa_*a_*)^{-1}.$$

(B) Insulated boundaries: $x=-L/2,L/2$:

$$\psi_i=\frac{\partial\psi_i}{\partial x}=0,\quad \frac{\partial T_i}{\partial x}=0,\quad i=1,2,3. \tag{2.6b}$$

The boundary value problem (2.1)–(2.6) contains 17 independent nondimensional parameters. The parametric investigation of this problem seems to be impossible. Because of this we shall concentrate on some particular systems of fluids demonstrating various characteristic phenomena.

The boundary value problem (2.1)–(2.6) was solved by the finite-difference method. Equations (2.1) were approximated on a uniform mesh using a second-order approximation for the spatial coordinates. The calculations were started with initial conditions corresponding to equilibrium fields of temperature and localized vorticity of different sign in several points (see Fig. 2). The nonlinear equations were solved using the explicit scheme, as a rule on a rectangular uniform 28×84 mesh. We checked up the results also on 42×84 and 28×126 meshes. The time step was calculated by the formula

$$\Delta t=\frac{[\min(\Delta x,\Delta y)]^2[\min(1,\nu,\chi,\nu_*,\chi_*)]}{2[2+\max|\psi_i(x,y)|]}.$$

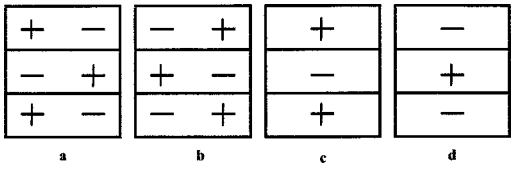

FIG. 2. Types of initial conditions for vorticity.

The Poisson equations were solved by the iterative Liebman successive over-relaxation method on each time step: the accuracy of the solution was fixed (10^{-4} for steady solutions and 10^{-5} for oscillations). The Kuskova and Chudov formulas [18] providing the second-order accuracy were used for approximation of the vorticity on the solid boundaries. For example, on the boundary $x=0$

$$\varphi_i(0,y)=\frac{\psi_i(2\Delta x,y)-8\psi_i(\Delta x,y)}{2(\Delta x)^2}.$$

At the interfaces the expressions for the vorticities at the exterior layers are approximated with second-order accuracy for the spatial coordinates and have a form

$$\varphi_3(x,0)=-\frac{2[\psi_2(x,-\Delta y)+\psi_3(x,\Delta y)]}{(\Delta y)^2(1+\eta)}-Mr\frac{1}{1+\eta}\frac{\partial T_3}{\partial x}(x,0), \tag{2.7}$$

$$\varphi_2(x,0)=\eta\varphi_3(x,0)+Mr\frac{\partial T_3}{\partial x}(x,0), \tag{2.8}$$

$$\varphi_2(x,-a)=-\frac{2[\psi_1(x,-a-\Delta y)+\psi_2(x,-a+\Delta y)]}{(\Delta y)^2(1+\eta_*\eta^{-1})}-Mr_*\frac{1}{1+\eta_*\eta^{-1}}\frac{\partial T_2}{\partial x}(x,-a), \tag{2.9}$$

$$\varphi_1(x,-a)=\eta_*\eta^{-1}\varphi_2(x,-a)+Mr_*\frac{\partial T_2}{\partial x}(x,-a). \tag{2.10}$$

Here Δx, Δy are the mesh sizes for the corresponding coordinates. The temperatures on the interfaces were calculated by the second-order approximation formulas:

$$T_2(x,0)=T_3(x,0)=\frac{[4T_2(x,-\Delta y)-T_2(x-2\Delta y)]+\kappa[4T_3(x,\Delta y)-T_3(x,-2\Delta y)]}{3(1+\kappa)}, \tag{2.11}$$

$$T_2(x,-a)=T_1(x,-a)=\frac{\kappa_*[4T_2(x,-a+\Delta y)-T_2(x,-a+2\Delta y)]+\kappa[4T_1(x,-a-\Delta y)-T_1(x,-a-2\Delta y)]}{3(\kappa+\kappa_*)}. \tag{2.12}$$

The same code was formerly used for calculation of convective flows in three-layer systems (see [11,19]). It turned out to be efficient for calculation of both stationary and oscillatory convection regimes. A good agreement between linear and nonlinear theories was observed.

Nevertheless, we performed some additional tests. The typical test results obtained for the system described in Sec. III A ($M=27\,500$, $G=0$) are shown in Tables I and II. These tables present the dependences of the oscillation period τ and the maximal value of stream function $(\psi_3)_{\max}$ in the upper layer on the mesh size (Table I) and the time step (Table II). Relative changes of stream function amplitudes for all mesh sizes do not exceed 3%. The maximal relative changes (up to 10%) were observed for the vorticity near the corner points where the vorticity field is not continuous.

III. COMBINED ACTION OF RAYLEIGH AND THERMOCAPILLARY MECHANISMS OF CONVECTION

First of all, we shall discuss the specific features of convection in three-layer systems in comparison with one-layer and two-layer systems.

In one-layer systems, the Marangoni convection in the absence of the surface deformation is always stationary. In two-layer systems, the Marangoni oscillations may arise [2], but only in some specific cases [20]. In three-layer systems, the interaction of the interfaces may lead to the appearance of new mechanisms of oscillatory instability. Formally, the critical Marangoni numbers for the stationary convection in a three-layer system satisfy a quadratic equation [19,21], which does not always have real solutions (in the case of one-layer and two-layer systems, the Marangoni number is

TABLE I.

Mesh sizes	τ	$(\psi_3)_{\max}$
28×84	0.284	5.679
42×84	0.284	5.724
28×126	0.284	5.707

TABLE II.

Time step	τ	$(\psi_3)_{\max}$
Δt	0.284	5.670
$\Delta t/2$	0.284	5.661
$\Delta t/4$	0.284	5.656

TABLE III.

		Rayleigh convection		
		Upper layer	Middle layer	Lower layer
Marangoni convection	Upper interface	*A*	*B*	*C*
	Lower interface	*D*	*E*	*F*

calculated from a linear equation). In many cases, the disappearance of the stationary instability is a sign of an oscillatory instability. That is why the oscillatory instability in three-layer systems is much more widespread than in two-layer ones [13,19,21,22].

There is another situation which may appear only in three-layer systems in the presence of both buoyancy and thermocapillary instability mechanisms. Each layer is characterized by its own local value of the Rayleigh number, that is why the buoyancy convection instability is realized usually only in one of the layers. Similarly, the thermocapillary instability may be produced mainly by one of the interfaces. In the case where the thermocapillary convection and buoyancy convection are generated mainly in different fluids, some kind of ''indirect'' interaction of instability mechanisms is observed. Several different situations are brought together in Table III. In the rest of Sec. III we shall consider phenomena corresponding to the listed types of interaction between Rayleigh and Marangoni convection mechanisms.

A. System 1

We start with the simplest case, where the buoyancy convection arises mainly in the middle layer, the thermocapillary convection appears mainly near the upper interface (case *B* in Table III), and only steady motions are realized in the system.

Let us consider the system air/silicone oil 10 cs/fluorinert FC70, which is characterized by the following set of parameters [13]: $\eta_*=6.8\times10^{-4}$, $\nu_*=1.12$, $\kappa_*=0.375$, $\chi_*=643$, $\beta_*=3.6$, $\eta=2\times10^{-3}$, $\nu=1.57$, $\kappa=0.196$, $\chi=228.4$, $\beta=3.27$, $\overline{\alpha}=0.5$, $P=0.707$ (system 1). The thicknesses of the layers are assumed to be equal: $a=a_*=1$, $L=2.5$, $s=1$ (heating from below). Both types of boundary conditions (2.6a) and (2.6b) are used.

First, let us consider the thermocapillary convection ($M\neq0$, $G=0$). The threshold values M_c for both heat-conductive and heat-insulated lateral boundary conditions turned out to be rather close ($M_c\simeq25\,000$). The motion takes place mainly near the upper interface.

One can expect that two kinds of thermocapillary motions are possible. The case where the temperature near the vertical walls is lower than that near the symmetry plane $x=0$ will be defined as the case of ''cold corners.'' The opposite situation will be called the case of ''hot corners.''

As the initial state, we used the temperature field corresponding to the mechanical equilibrium state which is characterized by a temperature gradient, directed perpendicularly to the interfaces, and two kinds of vorticity fields characterized by the two-vortex structure in each layer [see Figs. 2(a) and 2(b)]. For the first kind of initial state [type (a)] a ''hot corner'' motion appears at small values of *t*. The typical dependence of the maximal value of the stream function $(\psi_i)_{\max}$ on *t* ($i=1,2,3$) is shown in Fig. 3 [boundary conditions (2.6a)]. One can see a ''plateau'' in the stream function for all the layers in the region $15<t<30$ corresponding to a transient state, containing vortices with different signs [see Fig. 4(a)]. Small vortices corresponding to the ''cold corner'' motion appear spontaneously near the vertical walls. Finally, the corner vortices replace the structure produced by the initial conditions, and the system evolves to the same steady state as for the second kind of initial conditions. The spatial structure of this steady motion which does not depend on the initial state corresponds to the ''cold corner'' case [see Fig. 4(b)] and is almost insensitive to the growth of the Marangoni number.

In the case of heat-insulated lateral boundary conditions (2.6b), the evolution of the structure from the initial conditions (a) and (b), as well as the final structure of the stationary thermocapillary motion, are similar to those obtained in the case (2.6a). The intensity of the motion in the case (2.6b) is somewhat lower than in the case (2.6a) (see Fig. 5). In both cases, for relatively small values of *M* the maximal value of the stream function is achieved in the upper layer, while for large values of *M* it is achieved in the middle layer.

Let us remember that in the one-layer case [23] the flow along the surface towards the cold wall compresses the thermal gradient, thereby enhancing the flow. That is why the motion in the case of a cold corner turns out to be essentially more intensive than in the case of a hot corner. For an external horizontal temperature gradient on the surface, the problem was investigated in detail by Canright [24] (see also [25]). We consider here the case where the external temperature gradient is directed perpendicularly to the interfaces. The temperature gradient along the interface is nonzero only because of the convective motion. One could assume that both cases of the ''cold corner'' and the ''hot corner'' may be observed. However, because of the positive feedback for a thermocapillary motion in the case of a ''cold corner,'' the motion corresponding to the latter case turns out to be preferred. Let us note that in the case of well-conducting vertical boundaries, the vorticity is not continuous in the corner points [26].

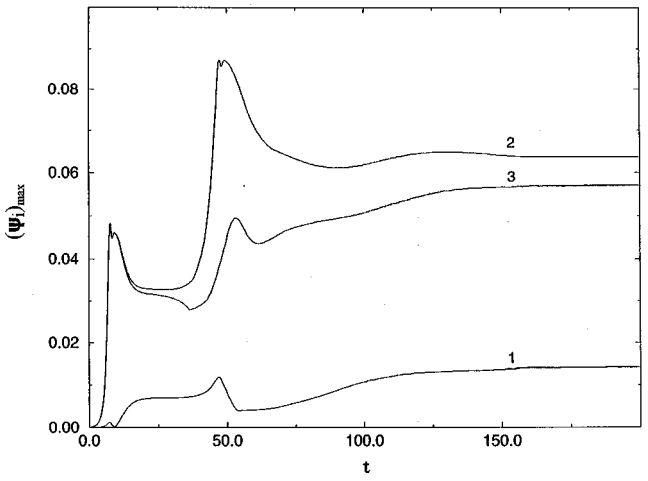

FIG. 3. Dependence of $(\psi_i)_{\max}$ ($i=1,2,3$) on *t* in the case of $M=40\,000$.

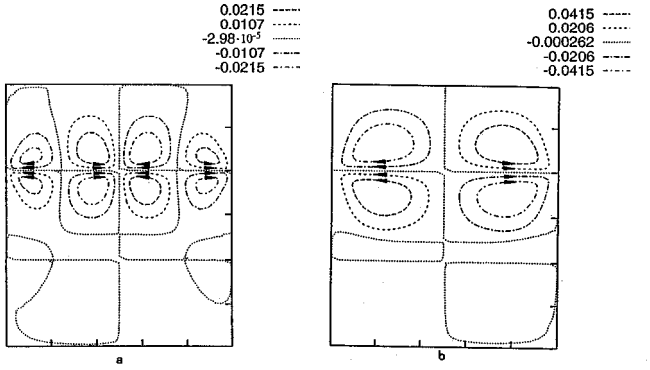

FIG. 4. (a) Transient state ($M=40\,000$); (b) streamlines of the steady motion for $M=40\,000$.

In the case of the buoyancy convection ($G\neq 0$, $M=0$), the motion appears mainly in the two lower layers [see Fig. 6(a)]. Let us note that the direction of the motion in the middle layer is the same in both cases of buoyancy and thermocapillary convection. That is why in the case $G\neq 0$, $M\neq 0$ the intensity of convection in the middle layer is larger under the action of both effects than in the absence of one of them [see Fig. 6(b)]. The situation is similar to that considered by Nield [27] for a one-layer system.

Thus, for system 1 the combined action of both mechanisms of instability, as well as the change of the lateral boundary conditions, do not produce qualitatively new flow structures.

For the system with the given physical properties it is possible to obtain a situation when the thermogravitational convection is realized mainly in the upper layer (case A in Table III). For this purpose we change the ratios of layer thicknesses: $a=a_*=0.4$; it means that the thickness of the upper layer is the largest one. Boundary conditions (2.6b) are used. In this case the direction of the vortices' rotation near the upper interface is the same both for buoyancy and thermocapillary convection and thermocapillary effect leads to the stabilization of the stationary instability mainly in the upper and middle layers. In the upper layer the motion has a two-story structure [see Fig. 6(c)].

B. System 2

In the present subsection, we shall concentrate on a qualitatively new situation, where both instability mechanisms act

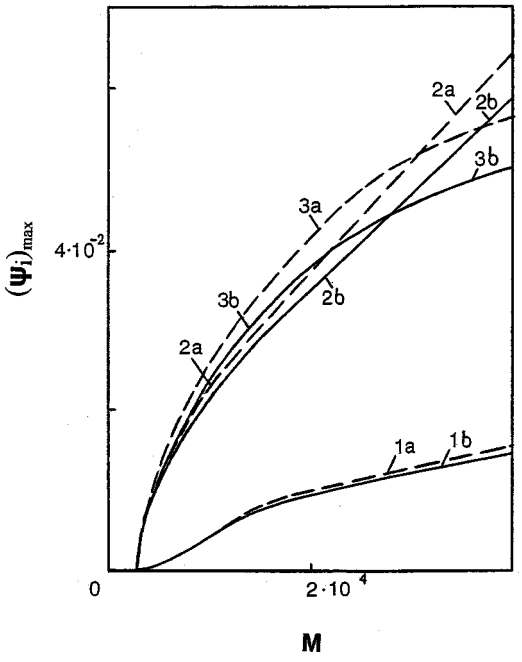

FIG. 5. Amplitude curves $(\psi_i)_{\max}(M)$ $(i=1,2,3)$ for (a) well-conducting and (b) heat-insulated lateral boundary conditions. The number of the line coincides with the number of the layer.

in different layers. Such an ''indirect'' interaction of instability mechanisms is possible only in three-layer systems.

Let us consider the system air/ethylene glycol/fluorinert FC75 which is characterized by the following set of parameters [28]: $\eta_*=0.013$, $\nu_*=18.767$, $\kappa_*=0.401$, $\chi_*=606.414$, $\beta_*=2.62$, $\eta=0.001$, $\nu=0.974$, $\kappa=0.098$, $\chi=215.1$, $\beta=5.9$, $P=0.72$, $\overline{\alpha}=0.08$. Let us take $a=a_*=1$, $L=2.5$, $s=1$. We use boundary conditions (2.6a). The diagram of structures is shown in Fig. 7. The pure buoyancy convection ($G\neq 0$, $M=0$) was considered formerly by Simanovskii [29]. We can introduce the Rayleigh numbers determined by the parameters of each layer:

$$R_i=\frac{g\beta_i A_i a_i^4}{\nu_i\chi_i},\quad i=1,2,3.$$

In our case the ''local'' Rayleigh numbers differ considerably:

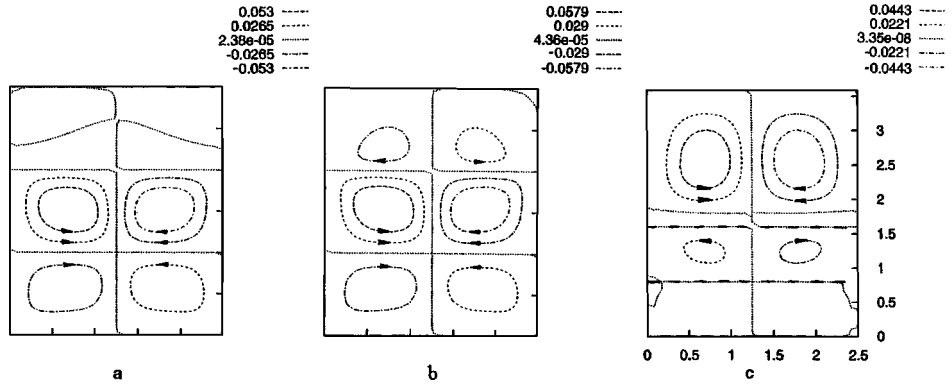

FIG. 6. Streamlines in the case of heat-insulated boundary conditions: (a) $G=1750$, $M=0$; $a=a_*=1$; (b) $G=1750$, $M=12\,000$; $a=a_*=1$; (c) $G=500$, $M=5000$; $a=a_*=0.4$.

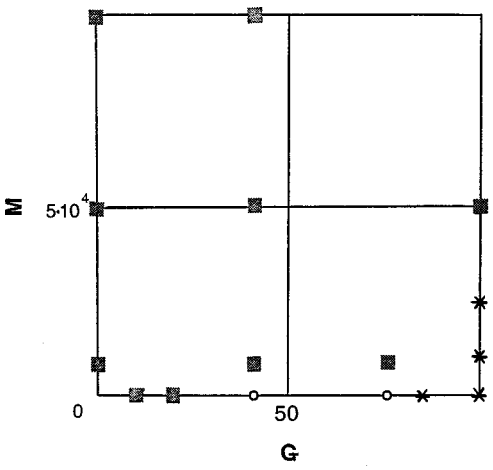

FIG. 7. Diagram of strucutres (■—structure *A*, ○—structure *B*,*—structure *C*).

$$\frac{R_2}{R_3}=3.5, \quad \frac{R_1}{R_3}=1.7\times 10^3.$$

Because of this, the intensive convection motion arises only in the lower layer ($G_c \simeq 2.5$); in the other layers weak induced motions exist (see Fig. 8). It is interesting that the structure of the motion changes with the increase in G. For relatively small G [see Fig. 8(a)] the fluid goes down in the middle of layer 1 (structure I). When G increases, the lateral vortices become stronger and suppress the central vortices, so that structure I is smoothly transformed into a steady four-vortex structure II [see Fig. 8(b)]. For large G [see Fig. 8(c)] the fluid goes up in the middle of layer 1 (structure III). There is a hysteretic transition between structures II and III: in the interval of the Grashof numbers $30<G<80$ the stability regions of these structures are overlapped. For all the configurations, the symmetry properties

$$\psi_i(x,y)=-\psi_i(-x,y), \quad T_i(x,y)=T_i(-x,y), \quad i=1,2,3 \tag{3.1}$$

are not violated. It is known (see [20,30,31]) that the bifurcation of steady finite-amplitude motions with the symmetry (3.1) is two sided (the motions with different direction of rotation are not equivalent; the preferred motion appears in a subcritical way). These details cannot be seen in the scale of the graph.

Let us consider now the case of the pure thermocapillary convection ($G=0$, $M\neq 0$; see Fig. 7). The Marangoni convection is generated mainly in the second and the third layers [see Fig. 9(a)]. In the third layer the fluid goes down in the middle part of the layer, in the second layer it goes up, and in the first layer it goes down [the latter motion is invisible in Fig. 9(a)].

Now we shall discuss the case of the combined action of buoyancy and thermocapillary mechanisms of convection ($G\neq 0$, $M\neq 0$; see Fig. 7). The considered system belongs to type *C* of Table III. Because the thermocapillary convection in the second and the third layers induces a descending flow in the middle of the first layer, it supports structure *A* against other possible structures. For nonzero values of M one can observe in the lower layer structure *A* [Fig. 9(b)] instead of both structures *B* and *C*. If M is nonzero but not sufficiently large, the structure *C* survives [see Fig. 9(c)]. In the latter case, some small vortices appear, separating mainly buoyancy convection motion in the lower layer and mainly thermocapillary motions in the middle layer and in the upper layer.

The considered example shows that the structure of the buoyancy convection in a certain layer may be influenced by thermocapillary convection appearing in some other fluid layers.

Let us change the ratio of layer thicknesses: $a=1$; $a_*=4$; it means that the lower layer has the largest thickness. The thermocapillary convection appears mainly near the upper interface [see Fig. 10(a)]. As for the given case $R_1>R_2>R_3$, the buoyancy convection is realized mainly in the lower layer. Let us note that nonlinear oscillatory convection is possible in that case [see Figs. 10(b) and 10(c)]. The oscillatory motion retains in the system under the combined action of both mechanisms of instability ($G\neq 0$, $M\neq 0$). The maximum values of stream function modulus in all the layers as a function of time are presented in Fig. 11. The evolution of the streamline patterns during one-half of the period is shown in Figs. 12(a)–12(d). The most intensive motion of the gravitational nature takes place in the lower layer, where

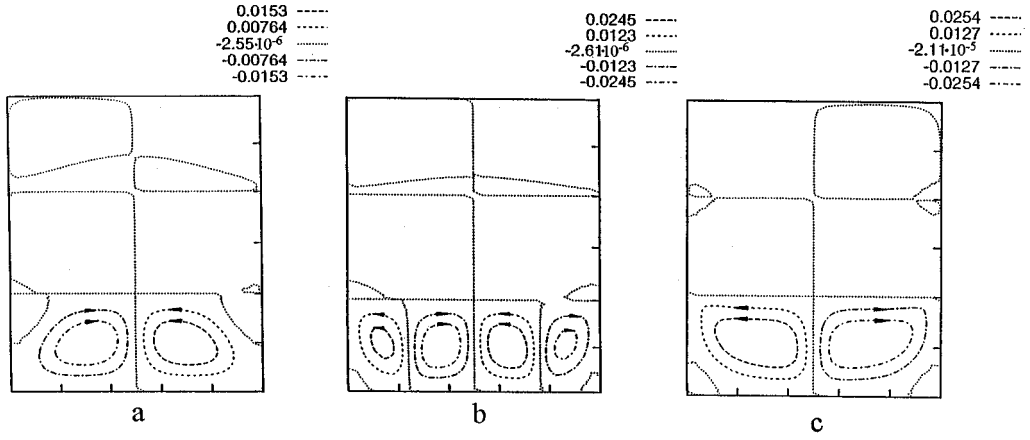

FIG. 8. Streamlines for $M=0$; (a) $G=20$, (b) $G=75$, (c) $G=100$.

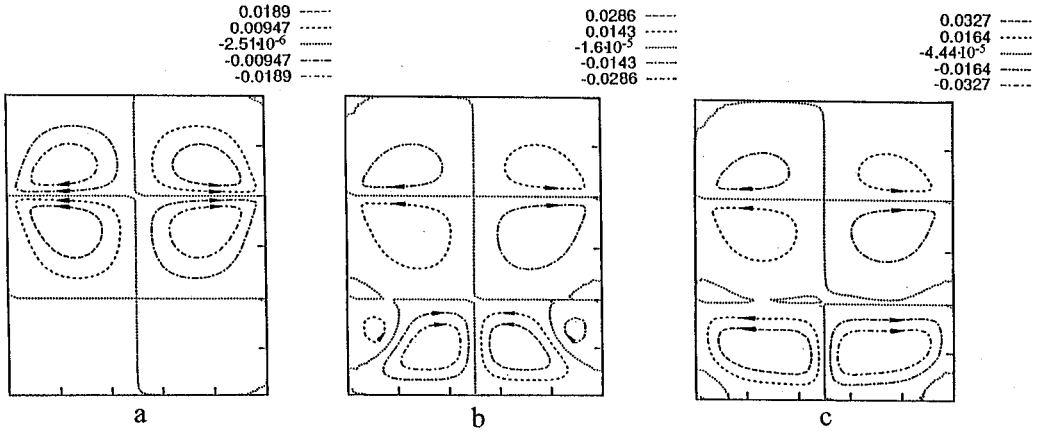

FIG. 9. Streamlines for the system air/ethylene glycol/fluorinert FC75 ($a=a_*=1$; $\bar{\alpha}=0.08$): (a) $G=0$, $M=50\,000$; (b) $G=75$, $M=25\,000$; (c) $G=100$, $M=25\,000$.

during one-half of the period the vortices change their signs. The thermocapillary motion in the upper and middle layers is weakly influenced by the buoyancy convection in the lower layer.

Now let us consider a case when the thickness of the middle layer is larger than the thickness of the exterior layers: $a=2.4$, $a_*=0.4$. The ratios of local Rayleigh numbers are

$$\frac{R_2}{R_3}=115.5, \quad \frac{R_1}{R_3}=44.6.$$

In this situation the intensive buoyancy convection ($G\neq 0$, $M=0$) arises mainly in the middle layer [see Fig. 13(a)]. The competition between the buoyancy convection and the thermocapillary effect (type *B* in Table III) intensifies the stationary motion [see Fig. 13(b)]. One can see that the maximum of the motion's intensity takes place in the middle layer, close to the upper interface.

Let us note that the increase of the ratio of the thermal coefficients of the surface tension $\bar{\alpha}$ (for example, by the addition of the surface-active agents on the interfaces) leads to the change of the ''activities'' of the interfaces. We shall take $a=a_*=1$. For $G=0$, $M\neq 0$, if $0.08<\bar{\alpha}<1$ the upper interface plays an active role in the generation of convection, if $1<\bar{\alpha}<4.5$ thermocapillary convection is generated by both upper and lower interfaces, and if $4.5<\bar{\alpha}<12.5$ the motion takes place mainly near the lower interface. In the last case inclusion of buoyancy convection ($G\neq 0$) leads to type *F* in Table III.

With the increase in $\bar{\alpha}$ the situation changes essentially also for the layers with unequal thicknesses. Let us take $a=2.4$, $a_*=0.4$, $\bar{\alpha}=12.5$. In this case the thermocapillary convection appears mainly near the lower interface, and, as was discussed above, the buoyancy convection arises mainly in the middle layer. It means that the system belongs to type *E* in Table III. The combined action of buoyancy and thermocapillary mechanisms ($G\neq 0$, $M\neq 0$) leads to the establishment of the steady motion mainly in the lower and

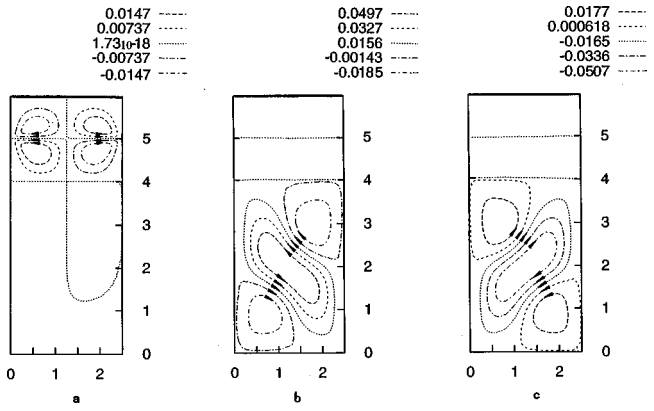

FIG. 10. Streamlines ($a=1$, $a_*=4$, $\bar{\alpha}=0.08$) for (a) steady thermocapillary convection ($G=0$, $M=60\,000$); (b), (c) oscillatory buoyancy convection ($G=5$, $M=0$).

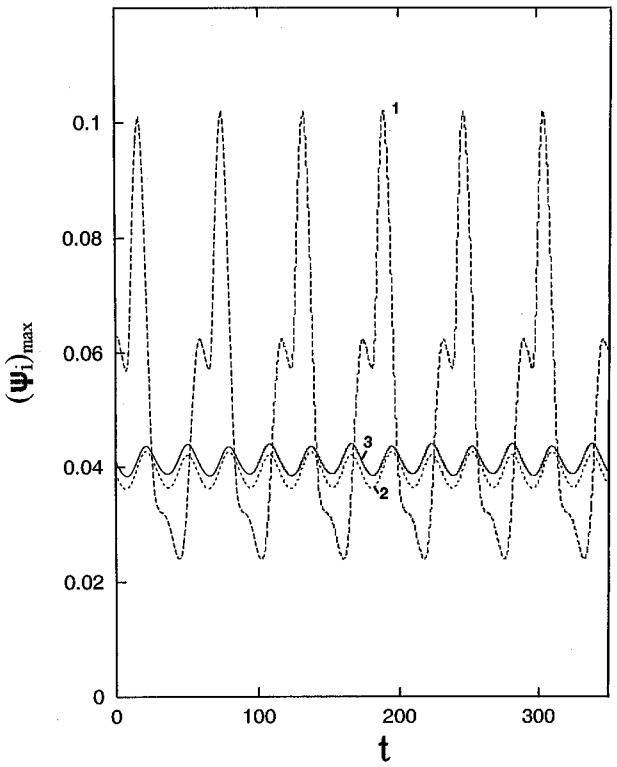

FIG. 11. Dependence of $|(\psi_i)|_{\max}$ ($i=1,2,3$) on t in the case $G=5$, $M=60\,000$; $a=1$, $a_*=4$, $\bar{\alpha}=0.08$.

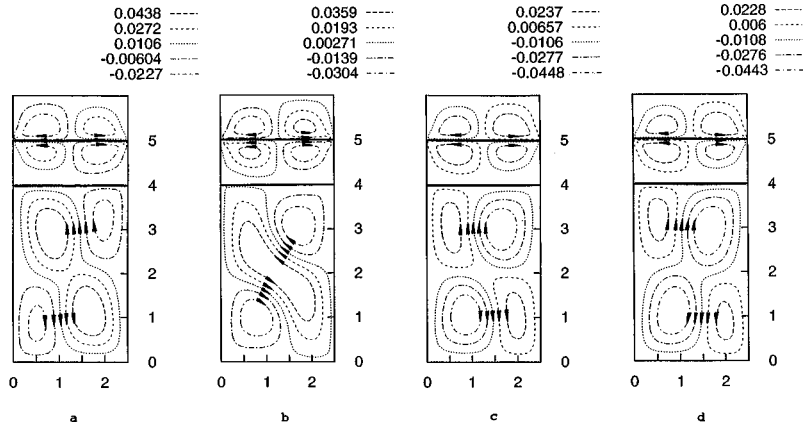

FIG. 12. Streamlines (a)–(d) for the periodic oscillatory motion for the half of the period $G=5$, $M=60\,000$; $a=1$, $a_*=4$; $\overline{\alpha}=0.08$.

middle layers close to the lower interface [see Fig. 13(c)].

Let us consider now the case when the thickness of the upper layer is larger than the thicknesses of the other layers: $a=0.333$, $a_*=0.133$. For $\overline{\alpha}=12.5$ the buoyancy convection is realized mainly in the upper layer and the thermocapillary convection appears mainly near the lower interface. In Table III such a situation is classified as type *D*. The combined action of both mechanisms of instability ($G\neq 0$, $M\neq 0$) leads to the arising of the steady motion in the system. As for ''pure'' thermogravitational convection, the most intensive motion takes place mainly in the upper layer.

C. Oscillatory convection regimes due to the interaction of interfaces

In the previous example, only one of the interfaces played an active role in the generation of the thermocapillary convection. To investigate the interaction between two active interfaces, we consider the model system, where all the parameters of fluids are equal except dynamic and kinematic viscosities: $\kappa=\kappa_*=\chi=\chi_*=a=a_*=\overline{\alpha}=1$, $\eta=\nu=0.5$, $\eta_*=\nu_*=0.25$. It means that the lowest layer has the highest viscosity. We choose $P=1$, $L=2.5$. We use boundary conditions (2.6a).

The general diagram of regimes is shown in Fig. 14.

Let $G=0$. From results of [19], we expect that thermocapillary oscillations may arise in the system, because of equal values of temperature diffusivities. It turns out that the mechanical equilibrium state is stable if $M<M_0=12\,700$ (see Fig. 14). As $M>M_0$, the equilibrium state becomes unstable with respect to oscillatory disturbances. This instability leads to temporally periodic oscillations (regime 1) which appear in a supercritical way. Let us describe qualitatively the flow evolution during the period of oscillations (see Fig. 15). We start from the state where an intensive thermocapillary convection corresponding to a ''cold corner'' configuration takes place mainly in the third layer and in the second layer, while the fluid in the first layer is almost stagnant [Fig. 15(a)]. The fluid motion in the second layer induces two weak vortices in the first layer [Fig. 15(b)]. Because the ascending flow in the middle of the second layer is more intensive than the descending flow in the first layer, a maximum of the temperature distribution appears in the middle point of the lower interface. As the result, the temperature field generates a new four-vortex structure in the first layer and in the second layer [see Fig. 15(c)] which ousts the former structure. An intensive motion developing in the second layer induces a motion in the opposite direction in the third layer [see Fig. 15(d)] and diminishes the temperature in

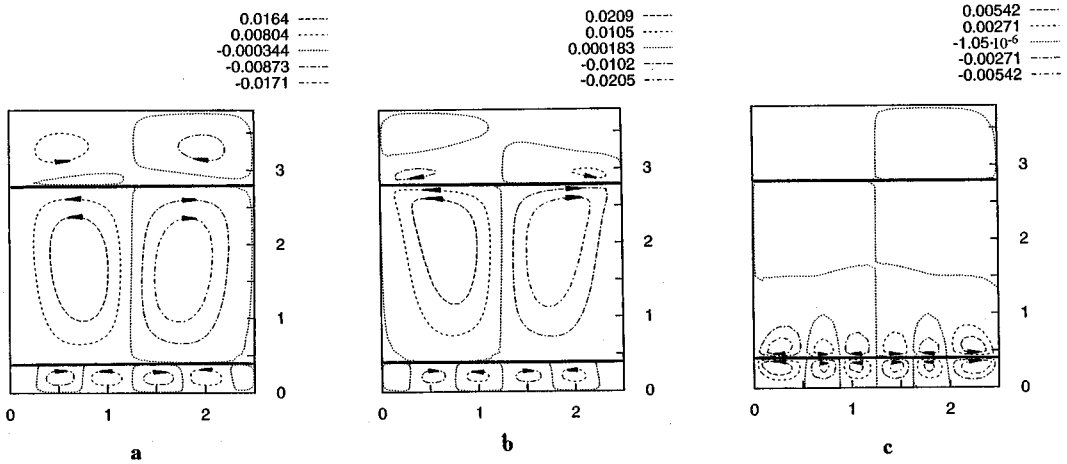

FIG. 13. Streamlines for the ratios of layer thicknesses $a=2.4$, $a_*=0.4$: (a) $G=240$, $M=0$; $\overline{\alpha}=0.08$; (b) $G=240$, $M=12\,000$; $\overline{\alpha}=0.08$; (c) $G=20$, $M=5000$; $\overline{\alpha}=12.5$.

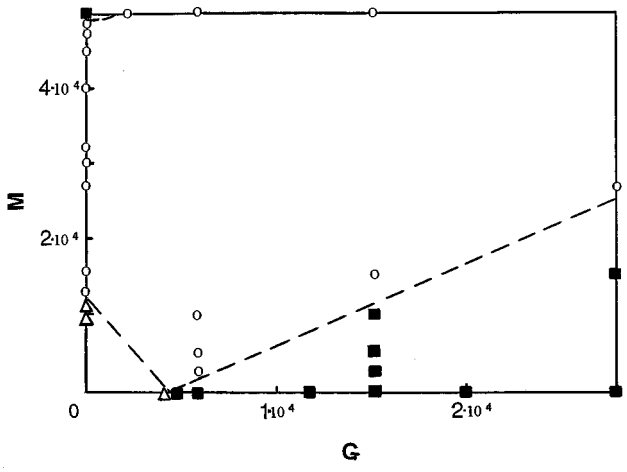

FIG. 14. The diagram of regimes (△—equilibrium, ■—steady state, ○—oscillations). The dashed lines separate the regions of different regimes.

the middle of the lower interface. Because of the latter phenomenon, the motion in the first layer slows down [Fig. 15(e)] and changes its direction [Fig. 15(f)]. A ''two-story'' structure appears in the second layer. The new growing vortices in the second layer suppress the upper pair of vortices [Fig. 15(g)], enhance the temperature in the middle of the upper interface, and diminish the temperature in the middle of the lower interface. That is why the flow in the first layer is suppressed [Fig. 15(h)], and finally the structure returns to the configuration of Fig. 15(a).

Thus, the main elements of patterns are mutually interacting four-vortex structures generated by temperature inhomogeneities on the interfaces that were analyzed formerly in [11,19].

To characterize the intensity and the structure of motions, we shall introduce the following integral characteristics:

$$S_l(t)=\int_{-L/2}^{0}dx\int_0^1 dy\ \psi_3(x,y,t),$$

$$S_r(t)=\int_0^{L/2}dx\int_0^1 dy\ \psi_3(x,y,t),$$

$$S_+=S_l+S_r,\quad S_-=S_l-S_r. \tag{3.2}$$

Near the threshold the oscillations have a rather simple, almost sinusoidal form (see Fig. 16, line 1), but the mean value of $S_l(t)$ is different from zero. The fields of stream function and temperature satisfy the symmetry conditions (3.1). For the symmetric motion (3.1), $S_r(t)=-S_l(t)$; thus, S_- oscillates, $S_+=0$. With the increase in the Marangoni number, the amplitude of oscillations grows (see Fig. 16, line 2), and their period τ decreases (see Fig. 17, line 1).

Let us note that the effect of the ''cold corner'' is observable also in the case of the oscillatory motion. In Fig. 18 the time evolution of the vorticity on the interfaces in the points $(x,y)=(L/2-\Delta x,0)$, $(x,y)=(L/2-\Delta x,-a)$, where Δx is the mesh size for the horizontal coordinate, is presented. The calculations were performed on the mesh 42×84. One can see that the sign of the vorticity is positive during almost the

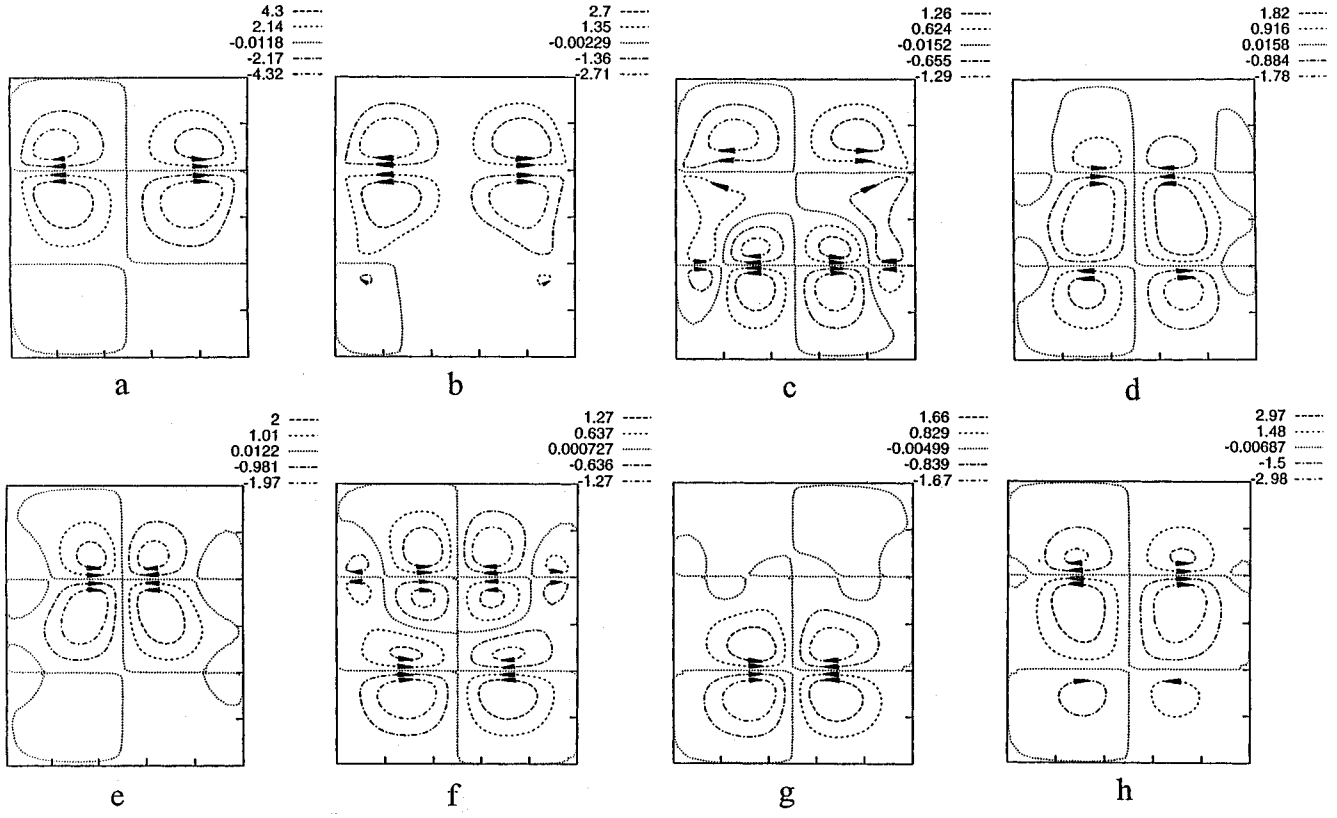

FIG. 15. Streamlines (a)–(h) for the periodic oscillatory motion at $M=27\,500$ for the whole period. Time interval between neighboring pictures is $\tau/8$.

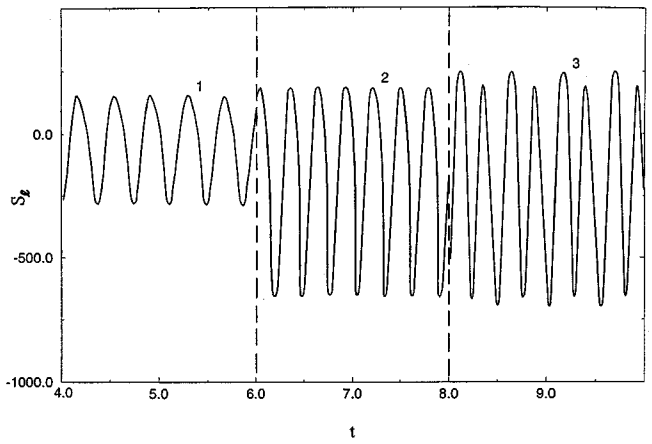

FIG. 16. Oscillations of $S_l(t)$ for the model system (line 1—$Mr=16\,000$, line 2—$M=27\,500$, line 3—$M=31\,200$).

whole period of oscillations. This sign of the vorticity corresponds to a ''cold corner'' motion. Let us note that the second harmonics caused by nonlinearity are much stronger in the oscillations of the vorticity in the corner than in the oscillations of the integral characteristics.

As $M \simeq 30\,500$, the symmetric oscillatory periodic motion becomes unstable with respect to disturbances violating the symmetry conditions (3.1). Now both variables S_- and S_+ are nonzero and oscillate. Generally, we could expect that the oscillations of S_+ would arise with a frequency incommensurable to the oscillation frequency of S_-. However, it turns out that a synchronization takes place: the oscillation frequency of S_- is exactly one-half of the oscillation frequency of S_+ (regime 2). Hence, one observes a *period doubling* (subharmonic bifurcation) of the limit cycle (see Fig. 19). The typical dependence $S_l(t)$ is shown in Fig. 16, line 3.

The time evolution of the stream function and temperature field during a half of the period is shown in Fig. 20. The general evolution of patterns is similar to one shown in Fig. 15, and its physical origin was explained above. Some pictures look similar [e.g., Fig. 15(c) and Fig. 20(e), Fig. 15(d) and Fig. 20(h), Fig. 15(e) and Fig. 20(i)]. However, the violation of the symmetry (3.1) is obvious during the main part of the period. In Figs. 20(k) and 20(l) the motion in the second layer is dominated by one strong vortex. In Figs. 20(a), 20(m), and 20(n) a one-vortex structure is observed in the third layer. Thus, the transition from regime 1 to regime 2 is connected with the competition of one- and two-vortex structures in the middle layer.

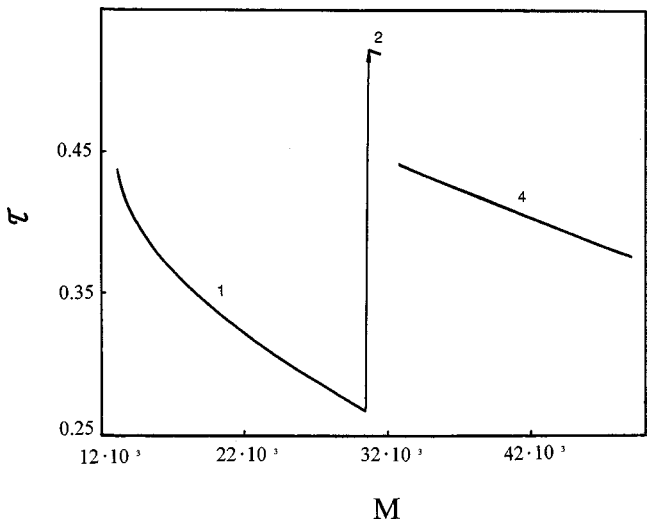

FIG. 17. Dependence of the period of oscillations τ on M for characteristic types of oscillations.

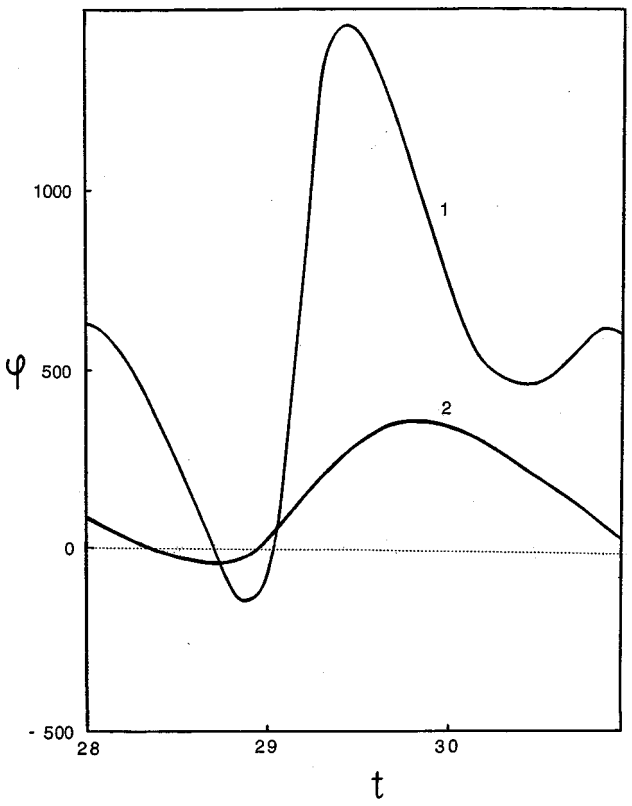

FIG. 18. Oscillations of vorticity for the whole period near the right corner on the upper interface (line 1) and lower interface (line 2); $M=27\,500$.

Comparing (a) and (n) in Fig. 20 one can see that

$$\psi_i(x,y,t+\tau/2) = -\psi_i(x,y,t), \tag{3.3}$$

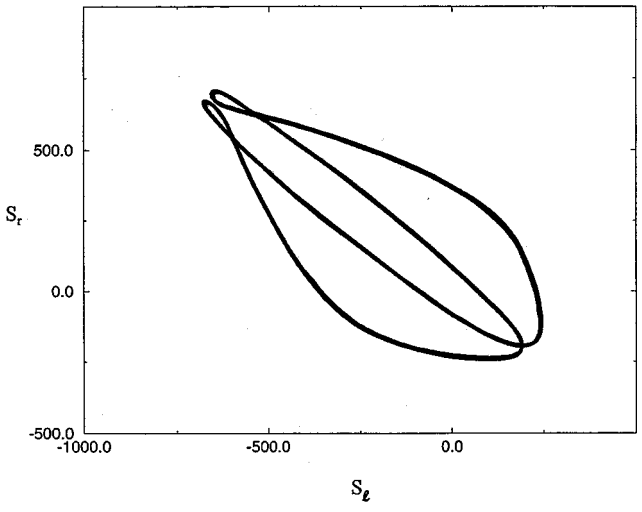

FIG. 19. Phase trajectory of the periodic motion after the period doubling bifurcation (regime 2, $M=31\,200$).

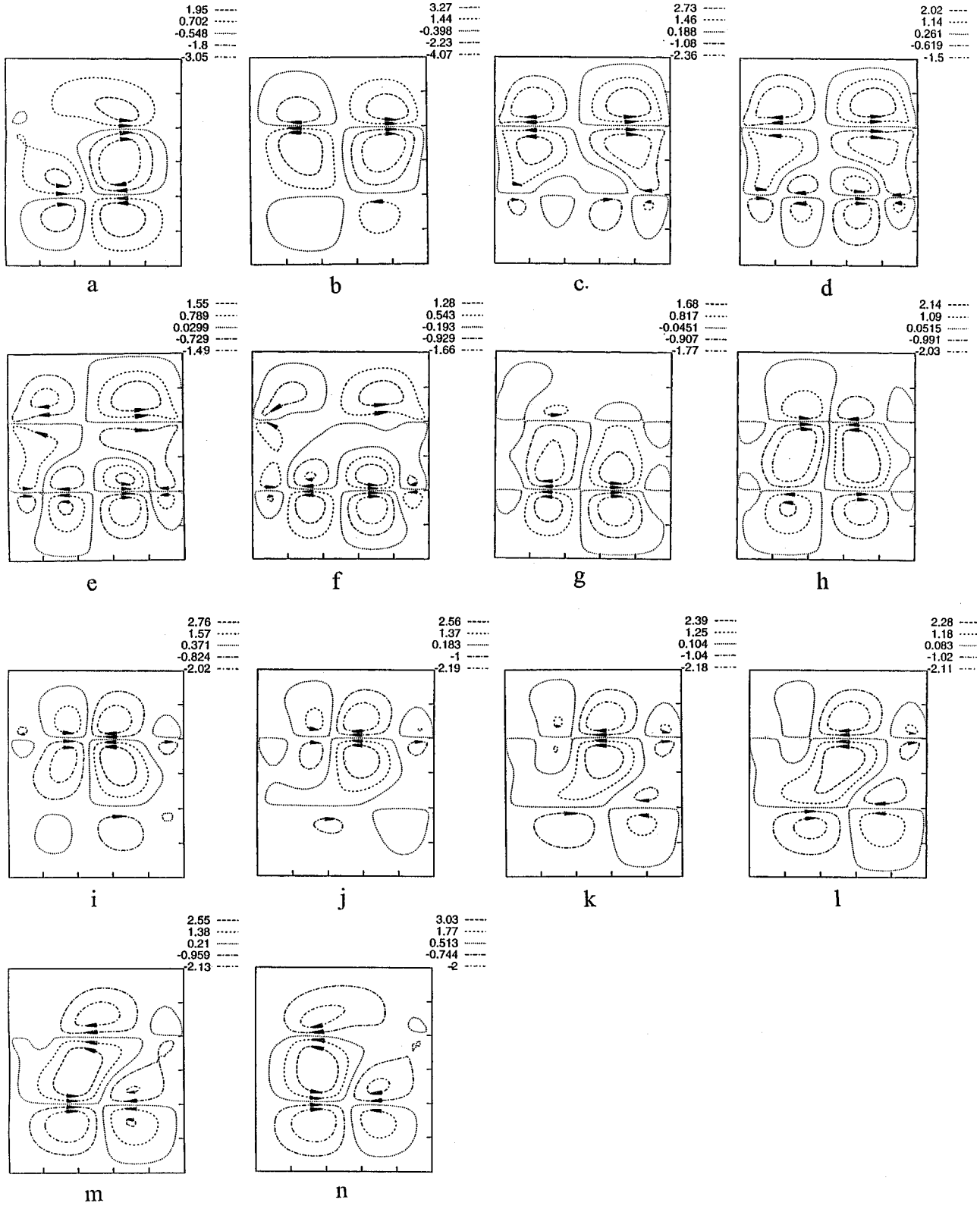

FIG. 20. Streamlines (a)–(n) for the periodic oscillatory motion at $M=31\,200$ for the half of the period.

$$T_i(x,y,t+\tau/2)=T_i(-x,y,t).$$

After the period doubling bifurcation, with the increase in M the period of oscillations decreases. For larger values of M the periodicity of the motion is destroyed; the phase trajectory is not closed (regime 3, see Fig. 21).

For $M>32\,000$ a new periodic regime is established (regime 4). The oscillations are strongly nonsinusoidal from the very beginning (see Fig. 22). The amplitude increases and the period decreases with the increase in the parameter M (see Fig. 17, line 4). These oscillations satisfy the same symmetry property (3.3) as ones for regime 2 (see Fig. 23), but

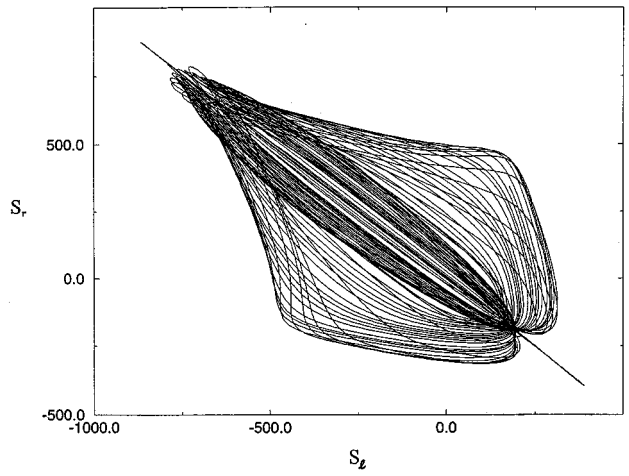

FIG. 21. Fragment of the phase trajectory of a nonperiodic motion (regime 3, $M=32\,000$).

the evolution of streamlines and isotherms is completely different (see Fig. 24). The four-vortex structures are absent; as a rule, there is only one main vortex in each layer. During one-half of the period, the vortex moves from the left to the right, then it is reflected by the lateral boundary and starts to move in the opposite direction. Recall that the pictures (a_1), (a_2) and (h_1), (h_2) are connected by the transformation (3.3). From the physical point of view, the transitions observed may be considered as a result of a competition between two instability modes: the ''symmetric'' mode satisfying condition (3.3), which leads to the development of regime 1, and the ''asymmetric'' mode leading to regime 4. In infinite layers, these modes would correspond to different values of the wave number. The nonlinear interaction of both modes generates more complicated regimes 2 and 3 which in some sense can be considered as a ''superposition'' of regimes 1 and 4. For $M\simeq 49\,960$ oscillations become unstable, and the steady motion satisfying symmetry condition (3.1) (regime 5) is established.

Let us consider now the case of the pure buoyancy convection (see Fig. 14) formerly studied by Simanovskii [29]. Obviously, the ratios of the ''local'' Rayleigh numbers are

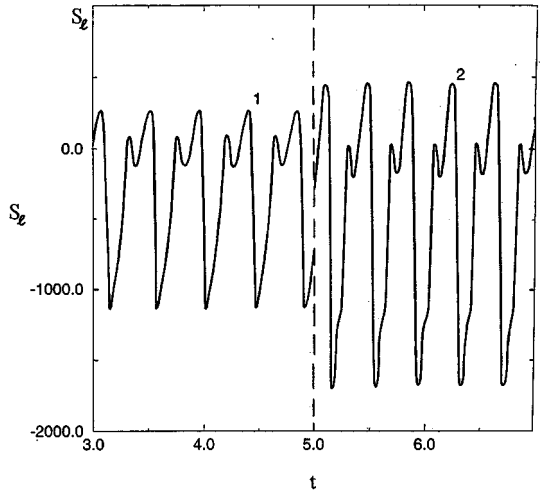

FIG. 22. Oscillations of $S_{\ell}(t)$ (line 1—$M=32\,350$, line 2—$M=47\,500$).

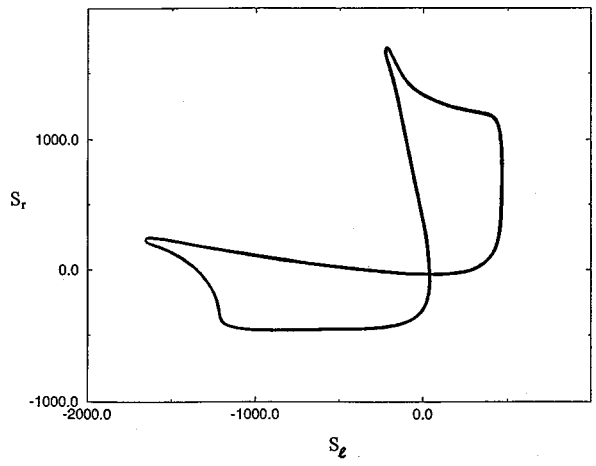

FIG. 23. Phase trajectory of the periodic motion (regime 4, $M=47\,500$).

$$\frac{R_2}{R_3}=0.5, \quad \frac{R_1}{R_3}=0.25.$$

Thus, the convection motion arises first of all in the upper layer (see Fig. 25); $G_c\simeq 5$. When the Grashof number is increased, the convection develops also in the middle layer and in the lower layer (see Fig. 26). The motions satisfy the symmetry conditions (3.1).

In the case where both thermocapillary and buoyancy mechanisms are present, it turns out that regime 4 is the preferred form of the motion. For instance, this oscillatory regime is observed for $G=15\,000$, $M=50\,000$ (see Fig. 14). Let us remember that for values of parameters $G=15\,000$, $M=0$ and $G=0$, $M=50\,000$ we obtained stationary motions. Another regime of oscillations which does not satisfy condition (3.3) was observed for $G=15\,000$, $M=16\,000$ (see Fig. 27).

IV. COMBINED ACTION OF THERMOCAPILLARY AND ANTICONVECTIVE MECHANISMS OF INSTABILITY

In the preceding section we considered several variants of the interaction between buoyancy and thermocapillary instability mechanisms acting by *heating from below*. If the system is *heated from above*, the usual Rayleigh instability mechanism is impossible, while the thermocapillary convection may appear. The thermocapillary instability mechanism may interact with the anticonvection formerly studied in [6–8].

We consider the model system with the following set of parameters: $\eta=0.2$, $\nu=1$, $\kappa=0.1$, $\chi=0.1$, $\beta=0.01$, $\eta_*=0.04$, $\nu_*=1$, $\kappa_*=0.1$, $\chi_*=0.07$, $\beta_*=0.01$, $\alpha=1$, $L=2.5$, $a=a_*=1$, $P=1$. It means that the heat expansion coefficient of the upper layer is much smaller than the heat expansion coefficient of the middle layer, and the thermal diffusivity of the middle layer is much higher than the thermal diffusivity of the upper one. This choice is based on the fact that this system displays an anticonvective instability when heated from above [29].

Let us explain the physical mechanism responsible for the anticonvective instability mode. Let a warm element of the third fluid move down towards the upper interface. Owing to

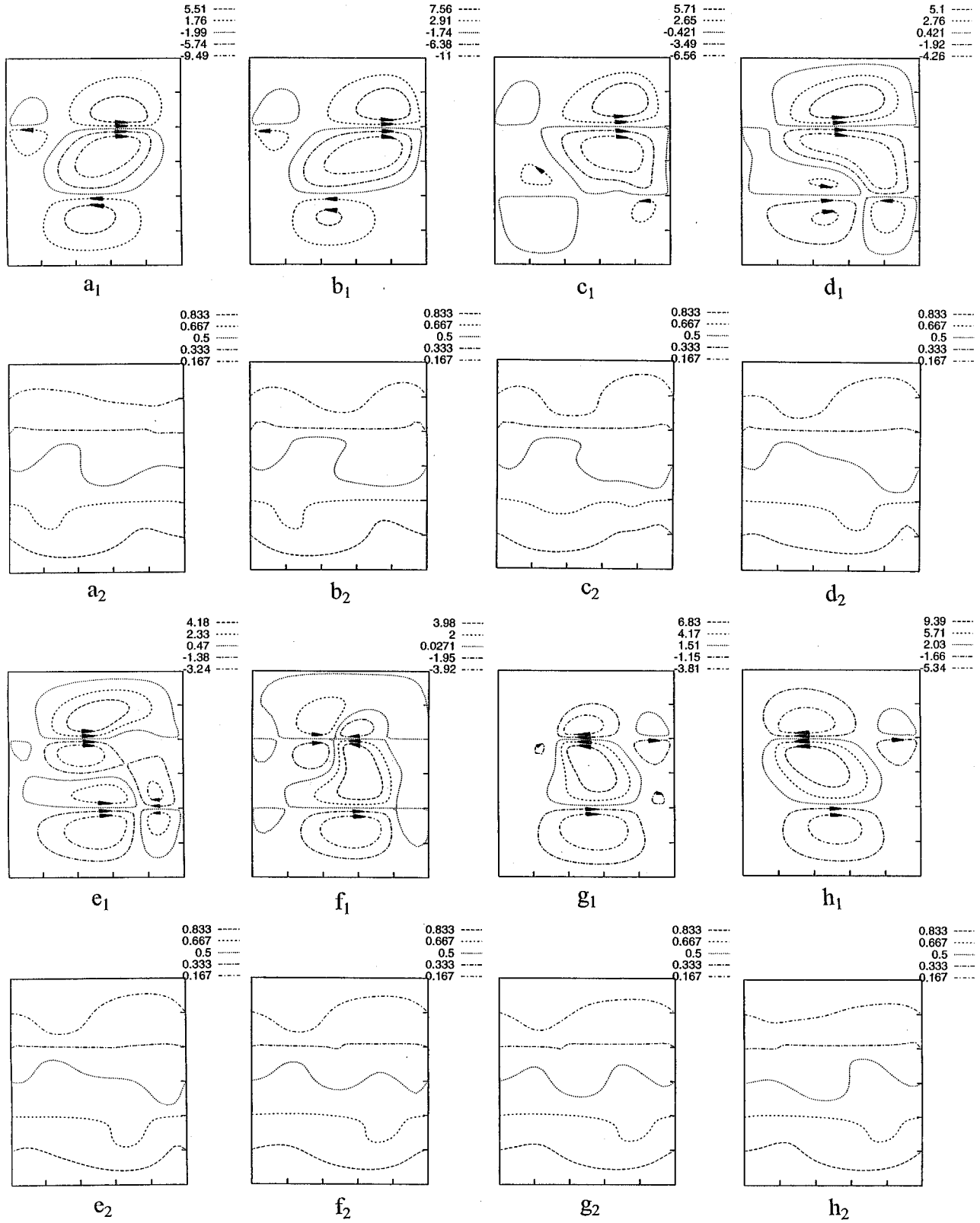

FIG. 24. Streamlines (a_1)–(h_1) and isotherms (a_2)–(h_2) for the periodic oscillatory motion at $M = 47\,500$.

the low thermal diffusivity of the upper layer ($\chi \ll 1$, $\chi_* \ll 1$) the element temperature remains higher than that of its ''neighbors'' for a long time. Since the heat expansion coefficient of the upper fluid is small ($\beta \ll 1$, $\beta_* \ll 1$) the Archimedian force does not act on this element, so that it can approach the interface. The change in the temperature field on the upper interface caused by the warm element leads to the appearance of temperature gradients directed along the interface to the spot under the element. These gradients cause the advective motion along the interface. Since the heat expansion coefficient of the middle layer is large, an ascending convective flow there arises. Because the thermal diffusivity

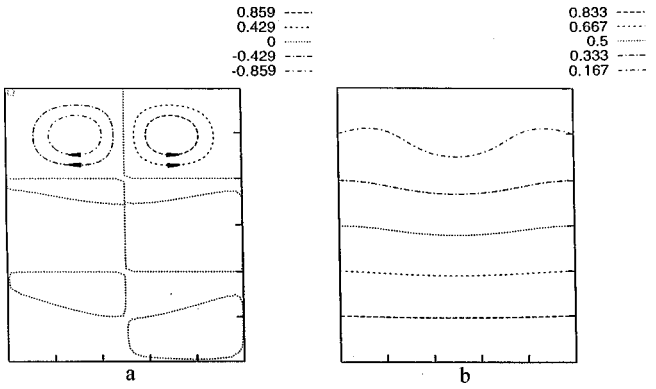

FIG. 25. Streamlines (a) and isotherms (b) for $G=6000$, $M=0$.

of the middle fluid is high, this flow does not destroy the warm spot. At the same time, the ascending motion in the middle layer supports a descending flow in the upper fluid by means of viscous stresses. Thus, a steady convective flow is generated.

For the system under consideration, conditions for the appearance of the anticonvection (as $G\neq 0$, $M=0$) are satisfied on the upper interface. As usual (see [20]), the intensity of the convection is maximal in the fluid situated below the active interface.

The thermocapillary convection ($M\neq 0$, $G=0$) also appears near the upper interface. Unlike the case of the anticonvection, the intensities of the thermocapillary convection in both upper and middle layers are of the same order [see Fig. 28(a)]. The directions of rotation coincide for anticonvective and thermocapillary motions. When both mechanisms of instability act simultaneously, the intensity of the motion increases in both fluids, but its increase in the middle layer is much stronger [see Fig. 28(b)]. With the change in α (all the other parameters being the same), the role of two interfaces in the generation of the thermocapillary convection also changes. If $1<\alpha<180$ thermocapillary convection is generated by both interfaces, and if $\alpha>180$ the motion takes place mainly near the lower interface. Inclusion of buoyancy convection ($G\neq 0$, $M\neq 0$, $\alpha>180$) leads to indirect interaction of instability mechanisms. The most intensive motion takes place in the middle layer near the lower interface [see Fig. 28(c)].

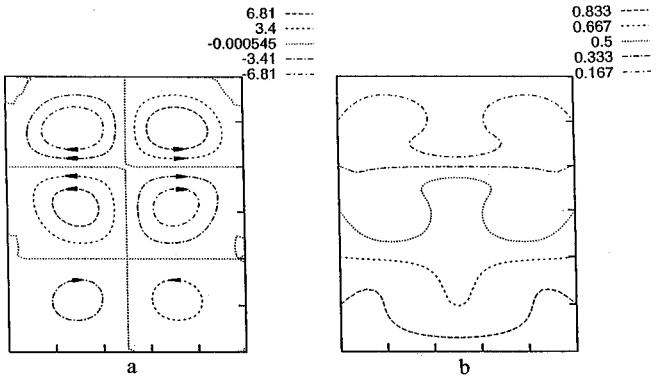

FIG. 26. Streamlines (a) and isotherms (b) for $G=28\,000$, $M=0$.

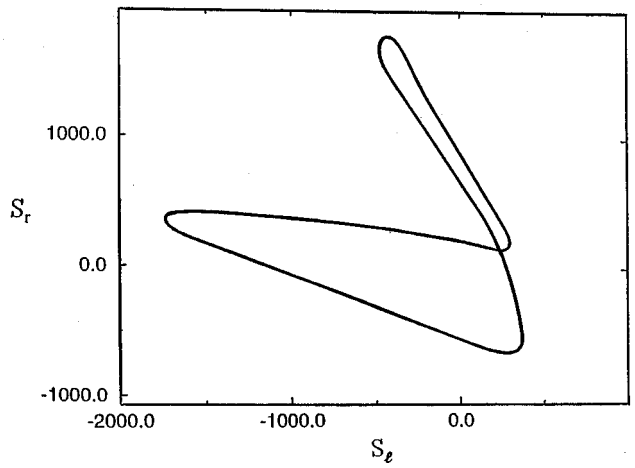

FIG. 27. Phase trajectory of the periodic motion ($G=15\,000$, $M=16\,000$).

V. CONCLUSIONS

We have considered the nonlinear regimes of thermocapillary and buoyancy convection and the combined action of several types of instabilities in three-layer fluid systems. The steady and oscillatory motions with different spatial structures and transitions between them were studied.

It was shown that for thermocapillary convection oscillations are restricted by the Marangoni number both from below (by the mechanical equilibrium state) and from above (by the steady state). The oscillations are subject to a transition between spatially symmetric and asymmetric forms. This transition is associated with a period doubling bifurcation. With the increase in the Marangoni number the period of oscillations decreases except for bifurcation points. In a finite interval of the Marangoni number nonperiodic oscillations are observed. Periodic oscillations take place both below and above this interval.

We have also investigated the influence of the lateral temperature boundary conditions on the convective motions. We found that this influence is rather weak; generally, the intensity of the motion is lower in the case of heat-insulated boundaries than in the case of well-conducting boundaries. Different variants of direct and indirect interactions of instability mechanisms are considered. In the simplest case, where only one of the interfaces plays an active role in the generation of the thermocapillary convection, the combined action of two instability mechanisms increases the intensity of motion. This effect is possible in one-layer and two-layer systems as well. However, for three-layer systems this interaction may be more delicate. In the case where there are several competing structures the interaction of different mechanisms may strongly influence the selection of the stable patterns. It was shown that the ''indirect'' influence of the thermocapillary effects on the motions generated mainly by buoyancy convection supports one particular structure over the other possible ones (for instance, structure *A* in Sec. III B). Similarly, buoyancy selects regime 4 among other oscillatory regimes of Marangoni convection (Sec. III C). We also found that the combined action of both instability mechanisms may produce a new regime of the motion (like that shown in Fig. 23) which cannot be generated by any sole mechanism. Classification of different types of interaction between Rayleigh and Marangoni convection mechanisms is

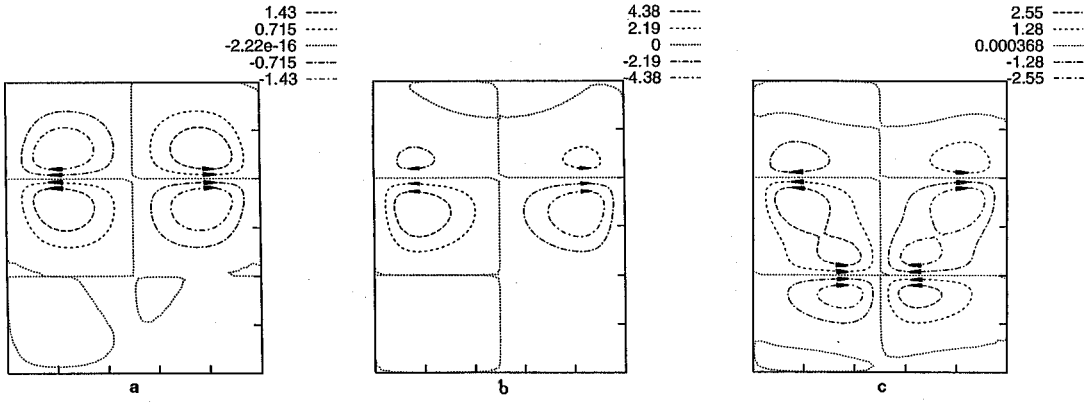

FIG. 28. (a) Streamlines for the model system ($M=12\,000$, $G=0$, $\alpha=1$); (b) streamlines for the model system ($M=12\,000$, $G=4500$, $\alpha=1$); (c) streamlines for the model system ($M=25\,000$; $G=4500$; $\alpha=200$).

suggested. All six types of interaction according to our classification are found.

ACKNOWLEDGMENTS

This work was supported by the Israel Science Foundation, Technion V.R.R. Fund–M. and M.L. Bank Mathematics Research Fund, and the Minerva Center for Nonlinear Physics of Complex Systems. I.B.S. acknowledges the support of the Israel Ministry of Science and Humanities and the Israel Ministry for Immigrant Absorption. The authors acknowledge I. Aranson whose help was crucial for the appearance of this work. I.B.S. is indebted to D. Kessler for fruitful discussions and constructive advice.

[1] J. R. Pearson, J. Fluid Mech. **4**, 489 (1958).
[2] C. V. Sternling and L. E. Scriven, AIChE. J. **56**, 514 (1959).
[3] J. J. Palmer and J. C. Berg, J. Fluid Mech. **51**, 385 (1972).
[4] E. Levchenko and A. Chernyakov, Sov. Phys. JETP **54**, 102 (1981).
[5] A. Nepomnyashchy and I. Simanovskii, Fluid Dyn. (USSR) **18**, 629 (1983).
[6] P. Welander, Tellus **16**, 349 (1964).
[7] G. Z. Gershuni and E. M. Zhukhovitskii, Fluid Dyn. (USSR) **15**, 816 (1980).
[8] I. B. Simanovskii, Ph.D. thesis, Leningrad State University, 1980.
[9] A. Yu. Gilev, A. A. Nepomnyashchy, and I. B. Simanovskii, Fluid Dyn. (USSR) **22**, 142 (1987).
[10] Ph. Georis and J.-C. Legros, in *Materials and Fluids Under Low Gravity*, edited by L. Ratke, H. Walter, and B. Feuerbacher (Springer, New York, 1995), p. 299.
[11] I. Simanovskii, Ph. Georis, M. Hennenberg, S. Van Vaerenberg, I. Wertgeim, and J.-C. Legros, in *Proceedings of the VIII European Symposium on Materials and Fluid Sciences in Microgravity*, edited by European Space Agency SP-333 (ESA Publiciations Division, Brussels, Belgium, 1992), p. 729.
[12] Q. S. Liu and B. Roux, in *Proceedings of the VIII European Symposium on Materials and Fluid Sciences in Microgravity*, Ref. [11], p. 735.
[13] Ph. Georis, Ph.D. thesis, Université Libre de Bruxelles, 1994.
[14] K. A. Smith, J. Fluid Mech. **19**, 321 (1966).
[15] M. Takashima, J. Phys. Soc. Jpn. **50**, 2745 (1981).
[16] S. J. Van Hook, M. F. Schatz, W. D. McCormick, J. B. Swift, and H. L. Swinney, Phys. Rev. Lett. **75**, 4397 (1995).
[17] A. A. Nepomnyashchy and I. B. Simanovskii, Q. J. Mech. Appl. Math. **50**, 149 (1997).
[18] T. V. Kuskova and L. A. Chudov, Comp. Meth. Programming **11**, 27 (1968).
[19] Ph. Georis, M. Hennenberg, I. Simanovskii, A. Nepomnyashchy, I. Wertgeim, and J.-C. Legros, Phys. Fluids A **5**, 1575 (1993).
[20] I. Simanovskii and A. Nepomnyashchy, *Convective Instabilities in Systems with Interface* (Gordon & Breach, London, 1993).
[21] V. Kats-Demyanets, A. Oron, and A. Nepomnyashchy, Eur. J. Mech. B/Fluids **16**, 49 (1997).
[22] J.-C. Legros and Ph. Georis, report.
[23] A. Zebib, G. M. Homsy, and E. Meiburg, Phys. Fluids **28**, 3467 (1985).
[24] D. Canright, Phys. Fluids **6**, 1415 (1994).
[25] V. M. Shevtsova, H. C. Kuhlmann, and H. J. Rath, in *Materials and Fluids Under Low Gravity*, edited by L. Ratke, H. Walter, and B. Feuerbacher (Springer, New York, 1996), p. 323.
[26] H. K. Moffat, J. Fluid Mech. **18**, 1 (1964).
[27] D. A. Nield, J. Fluid Mech. **19**, 341 (1981).
[28] A. Prakash and J. N. Koster, Eur. J. Mech. B/Fluids **12**, 635 (1993).
[29] I. B. Simanovskii, Physica D **102**, 313 (1997).
[30] A. Nepomnyashchy and I. Simanovskii, in *Hydrodynamic and Convective Stability of Incompressible Fluid*, edited by V. Briskman and E. Tarunin (USC AS USSR edition, Sverdlovsk, 1984), p. 10.
[31] K. H. Winters, Th. Plesser, and K. A. Cliffe, Physica D **29**, 387 (1988).